

EMBEDDING KADANOFF'S SCALING PICTURE INTO THE TRIANGULAR LATTICE*

DOMINIQUE DÉSÉRABLE

Institut National des Sciences Appliquées
Laboratoire de Génie Civil et Génie Mécanique
20 Avenue des Buttes de Coësmes, 35043 Rennes, France
`deserable@insa-rennes.fr`

(Received April 6, 2011)

A strictly topological aspect in renormalization theory is tackled from Kadanoff's scaling picture which splits the square lattice into nested blocks and we study how to embed similar schemes onto the triangular lattice. From a preliminary study on the various ways of splitting the dual honeycomb into polyhexes while preserving symmetries, it is shown that only two patterns are relevant: either a 3-hex prototile or a 4-hex prototile. The first one has been investigated in detail by Niemeijer and van Leeuwen. The other alternative leads to an "arrowhead picture" and is the core of our proposal. As far as we know, the resulting spin lattice has never been investigated elsewhere. It should be pointed out that these scaling pictures differ from exactly solved models and in particular from the star-triangle transformation.

DOI:10.5506/APhysPolBSupp.4.249

PACS numbers: 02.10.Ox, 05.50.+q, 05.10.Cc

1. Introduction

The renormalization methods appeared these last forty years in the area of statistical physics and dynamical systems. They apply quite well to the study of large scale *homogeneous systems*, illustrated by the image of the "chessboard" whose side, of length L , represents the macroscopic scale while the square of the chessboard, whose side is of length $\xi \ll L$ and where ξ is the "correlation length", represents the mesoscopic scale which defines a homogeneous subsystem. These systems are thus characterized by a translational invariance by a vector of modulus ξ , namely, they are periodic. The renormalization methods have especially proven their efficiency in the study of critical phenomena where classical methods are shown to be unsuccessful —

* Presented at the 2nd Summer Solstice International Conference on Discrete Models of Complex Systems, Nancy, France, June 16–18, 2010.

at least until novel exact methods arise. A *critical system* is characterized by a scale invariance whose effect is a self-similar behaviour and a divergence of the correlation length at the critical point $\theta = \theta_c$ of the control parameter. Usually, the divergence follows a power law (or “scaling law”) of the form $\xi(\theta) \approx (\theta - \theta_c)^{-\nu}$, where ν is the critical exponent. The same goes for the correlation length as well as for any thermodynamic quantity expressed in terms of the deviation $\theta - \theta_c$ bearing a specific critical exponent. It is up to the renormalization methods to deduce the value of these exponents, and thereby the behaviour of the system in a critical situation from only the property of scale invariance. By relying upon the self-similarity of the system, a way is to split it into nested blocks and to yield local averages in each of them (Kadanoff’s construction [1]). The long-range correlations remain unchanged after a sequence of transformations only if the system lies in a critical state. The operator defines a “renormalization (semi-)group” — in the algebraic meaning — and the sequence converges in that case towards a non-trivial fixed point [2,3,4,5]. The reader may refer to a plentiful literature (*e.g.* [6,7,8,9]) as well as very accessible digests (*e.g.* [10]) for a general review on renormalization methods and statistical mechanics.

We focus here on the *topological* aspect of the problem of scale change underlying this method. From Kadanoff’s “scaling picture”, we examine similar schemes iterated on the triangular lattice. Although Kadanoff construction, from a *strictly* topological standpoint, is straightforward in the (4-valent) orthogonal lattice, it is far from being so in the (6-valent) triangular one. For this reason, we first give an insight onto the various ways of tiling the plane from a primitive template, or “polyhexe” of size p (a p -hexe) in the hexagonal tessellation, the dual of which being the triangular lattice. It will be easy to show that tiling the plane with polyhexes of minimal size and with maximal symmetry, two requirements for simplifying a Kadanoff-like renormalization as much as possible, leads to only both prototiles: either a 3-hexe like in the Niemeijer–van Leeuwen construction or a 4-hexe as it is proposed herein.

It should be pointed out that Kadanoff’s approximation differs from *exactly* solved models and in particular from the star-triangle transformation, including the direct formulation of the duality relation in the partition function (see [11] and references therein) or the real-space renormalization in differential form (*e.g.* [12]).

After a recall of Kadanoff’s construction in Sec. 2, we highlight in Sec. 3 the two ways of tiling the honeycomb adequately by a suitable “prototile”. The Niemeijer–van Leeuwen scaling picture is described in Sec. 4 and the core of our proposal in Secs. 5–6. This work is an extension of a previous study related to cellular automata and presented elsewhere [13].

2. Kadanoff's construction

Kadanoff's scaling picture [1] (see also [5, 2, 10, 7]) defined on an orthogonal lattice of spins for the Ising model is displayed in Fig. 1, where the length a separating two neighbouring sites is the minimal scale. The validity of the construction comes from the fact that the interactions are short-range, which allows us to consider only the nearest-neighbour interactions. Each spin, associated to a site, has a proper energy (\uparrow) or (\downarrow) depending on the external magnetic field and each pair of neighbours, associated to a bond, has an interaction energy depending on whether they point towards the same direction or not. The calculation of the energy of the global configuration is renormalized by forming square blocks, or "cells", of 2×2 sites (Fig. 1 (a)) and yielding a local average according to a majority rule (the block has an arbitrary size but should contain a small number of sites and size 2×2 is usually chosen in the construction). Each block is then likened to a single "spin" at the upper scale of length $2a$ and the lengths are contracted by a factor 2 to maintain the initial density of the sites (Fig. 1 (b)). The construction is thus iterated until the correlation length ξ of the system in critical state is reached.

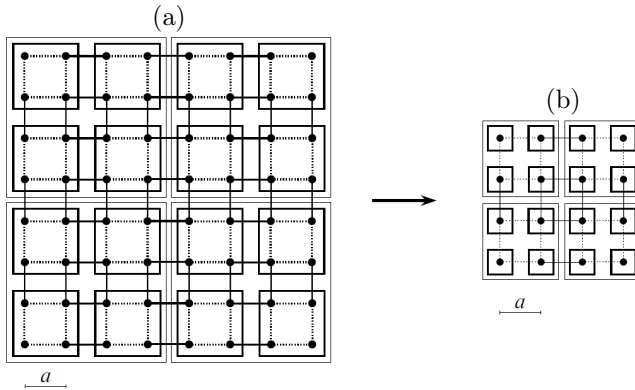


Fig. 1. Kadanoff's construction on the orthogonal lattice: dotted lines stand for inner interactions within a block, full lines for interactions between neighbouring blocks (after Lesne [7]).

We just focus on the graph transformation induced by the contraction. Let us denote the lattice, of finite size but toroidal, of Fig. 1 (a) by $\mathcal{K}_n = (V_n, E_n)$ of order $N = |V_n| = 2^n \times 2^n$. A vertex¹ (i, j) is connected horizontally to $(i \pm 1, j)$ and vertically to $(i, j \pm 1)$, where $0 \leq i, j < 2^n$ and the addition is modulo 2^n . Since the torus is 4-regular, the number of edges

¹ A vertex (resp. an edge) in the graph stands for a site (resp. a bond) in the lattice but no confusion is to be feared.

standing for the nearest-neighbour interactions is clearly $|E_n| = 2N$ (the wrapped edges are not displayed). In fact, periodic boundary conditions may be considered in the thermodynamic limit $N \rightarrow \infty$.

From these notations, the Hamiltonian of the model has the form

$$\mathcal{H} = -J \sum_{E_n} \sigma_{ij} \sigma_{i'j'} - h \sum_{V_n} \sigma_{ij}, \tag{2.1}$$

where $\sigma_{ij} = \pm 1$ is the value of the spin of site (i, j) and h denotes the magnetic field and where $((i, j), (i', j'))$ are neighbouring sites and J denotes the energy of a nearest-neighbour interaction. We will consider the reduced form

$$\mathcal{H} = K \sum_{E_n} \sigma_{ij} \sigma_{i'j'} \tag{2.2}$$

in a zero magnetic field $h = 0$ and where K is the normalized coupling constant associated to J and in which temperature and Boltzmann constant are absorbed. In this case, lattice \mathcal{K}_n is nothing but a signed graph and the partition function, from which all thermodynamic functions are deduced, is given by

$$\mathcal{Z}_N = \sum_s \exp(\mathcal{H}(s)), \tag{2.3}$$

where the summation is over all states s of the system.

The Hamiltonian may also take the form

$$\mathcal{H} = K_1 \sum_{E_n^{(1)}} \sigma_{ij} \sigma_{i'j'} + K_2 \sum_{E_n^{(2)}} \sigma_{ij} \sigma_{i'j'} \tag{2.4}$$

in the case where no isotropy is assumed: K_1 and K_2 become the horizontal and vertical coupling constants associated to the respective subsets $E_n^{(1)}$ and $E_n^{(2)}$ of E_n . This form will be ignored in the sequel, unless mentioned otherwise.

In Fig. 1 (a), the lattice is divided into $N_B = 4^{n-1}$ blocks of $l^d = 2 \times 2$ sites $(2i, 2i + 1) \times (2j, 2j + 1)$ with $0 \leq i, j < 2^{n-1}$ (l is the stretch factor and d the dimension). The edge set E_n is partitioned into a subset E'_n of “inner bonds” within a block (in dotted lines) and a subset E''_n of “outer bonds” between neighbouring blocks (in full lines). Thus

$$|E'_n| = 4N_B, \quad |E''_n| = |E'_n| \Rightarrow |E'_n| + |E''_n| = 2N = |E_n|. \tag{2.5}$$

Since the contraction shrinks a 2×2 block into a single “spin” and a pair of outer bonds into a single “bond”, that yields the new, renormalized lattice

$\tilde{\mathcal{K}}_n = (\tilde{V}_n, \tilde{E}_n)$ in Fig. 1 (b) isomorphic to \mathcal{K}_{n-1} , of order $\tilde{N} = N_B = |V_{n-1}|$, where

$$\tilde{E}'_n = \emptyset, \quad |\tilde{E}''_n| = \frac{1}{2} |E''_n| = 2N_B = |E_{n-1}| \tag{2.6}$$

and finally

$$\tilde{V}_n \cong V_{n-1}, \quad \tilde{E}_n = \tilde{E}''_n \cong E_{n-1}. \tag{2.7}$$

To be really precise, the renormalized lattice $\tilde{\mathcal{K}}_n$ is isomorphic (\cong) by a homothety of ratio 2 to the *dual* lattice² whose vertex set \tilde{V}_n is the centre set of the N_B blocks.

After shrinking, the new Hamiltonian has the similar form

$$\tilde{\mathcal{H}} = \tilde{K} \sum_{\tilde{E}_n \cong E_{n-1}} \tilde{\sigma}_{ij} \tilde{\sigma}_{i'j'}, \tag{2.8}$$

where $\tilde{\sigma}_{ij} \tilde{\sigma}_{i'j'}$ are all pairs of the block-spin variables and \tilde{K} is the new, renormalized coupling constant; the isomorphic mapping $\tilde{\mathcal{K}}_n \mapsto \mathcal{K}_{n-1}$ denotes the shrinking reduction of Fig. 1 (b). In Kadanoff's assumption, an *homogeneous* transformation on *analytic* functions of the form

$$\mathcal{F}(K) = l^{-d} \mathcal{F}(\tilde{K}) = \frac{\tilde{N}}{N} \mathcal{F}(\tilde{K}), \tag{2.9}$$

$$\xi(K) = l \xi(\tilde{K}) \tag{2.10}$$

is expected on all thermodynamic quantities such as the free energy \mathcal{F} and the correlation length ξ which do not depend of the lattice spacing a ! Their (universal) critical exponents will thus be obtained from a non-trivial fixed point

$$\tilde{K} = K^* \tag{2.11}$$

reached near the critical temperature T_c .

3. Tiling the plane with polyhexes

There exist multiple ways of arranging a grid network into a torus. In fact, any tiling of the plane formed by the assembly of copies of a ‘‘primitive’’ piece of elementary tiles, or *prototile*³, induces a compatible torus

² For a strict definition of ‘‘duality’’, refer to the following section.

³ Respectively *polyiamond*, *polyomino*, *polyhexe* (or *n-iamond*, *n-omino*, *n-hexe*) according to the regular (triangular, square, hexagonal) tessellation $\{3, 6\}$, $\{4, 4\}$, $\{6, 3\}$ of the plane, where $\{p, q\}$ is the Schläfli symbol [14, 15]. The Schläfli symbol gives a precise definition of a regular tiling; in particular the dual of $\{p, q\}$ is $\{q, p\}$ and *vice versa*.

by duality [16, 17]. For an illustration of this problem, see the example of polyominoes tiling the plane in the $\{4, 4\}$ tessellation and leading to a “double-loop” circulant graph [18].

Let us observe now an usual but similar construction in the hexagonal $\{6, 3\}$ case, borrowed from [19] and [20].

Each vertex i is connected with vertices $i \pm a, i \pm b, i \pm c$, where a, b, c are the three generators satisfying $a + b + c = 0 \pmod n$. A simple example is displayed in Fig. 2 with $n = 7$ and $(a, b, c) = (1, 2, 4)$, showing the tiling with polyhexes (a), its associated torus (b) and its triple-loop circulant graph (c) whose edge set can split into three edge-disjoint loops corresponding with the three generators and whose adjacency matrix is a circulant matrix.

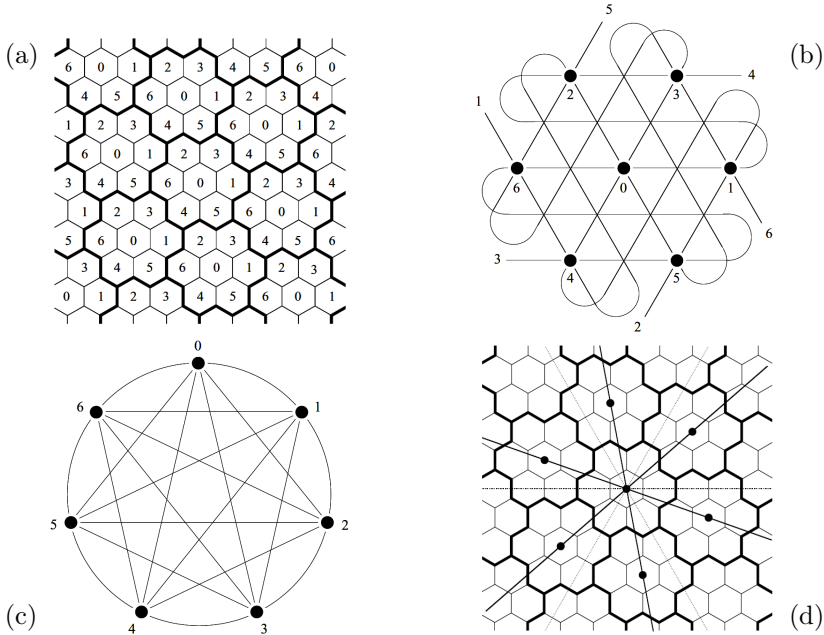


Fig. 2. (a) Tiling the plane with polyhexes. (b) Associated torus. (c) Associated triple-loop circulant graph. (d) Symmetry axes of the tiling.

Indeed, this minimal construction may appear as a particular case leading to the complete graph K_7 in Fig. 2(c), but the reader could easily deal with a 19-hex by adding a 12-ring surrounding this 7-hex prototile, and so forth. The order N_D of the circulant graphs which belong to this triple-loop family is clearly $N_D = 3D^2 + 3D + 1$, where $D = 0, 1, 2, 3 \dots$ is their diameter. Although circulant graphs may have nice properties, our main observation is that the symmetry axes in the elementary $\{6, 3\}$ tessellation and the symmetry axes induced by the prototile do not coincide, as shown in Fig. 2(d).

We try now to find a polyhexe of size p fulfilling Kadanoff's requirement, in other words, one should have a small size and preserves the implicit symmetry. Moreover, in order to simplify the Hamiltonian in a block-spin transformation, we require that the polyhexe must be both of minimal size and with maximal symmetry. Fixing $p < 7$, it would be easy but tedious to show that any p -hexe with $p = 2$, $p = 5$ or $p = 6$ must be eliminated. The remaining symmetric cases, displayed in Fig. 3, wherein $p = 3$ and $p = 4$, will yield respectively the pattern of Niemeijer–van Leeuwen and our own. It can be already observed that the 3-hexe in (a) is centred at the junction point of the three hexagons and will generate a new hexavalent lattice by a homothety of ratio $\sqrt{3}$, rotated by $\pi/2$ (or $\pi/6$) and shifted by $\sqrt{3}/3$; their construction is described hereafter. On the other hand, the centre set of the 4-hexes in (b) is the image of the initial vertex set by a homothety of ratio 2 *stabilizing* the symmetry axes, namely neither rotated nor shifted; the construction is presented in Sec. 5.

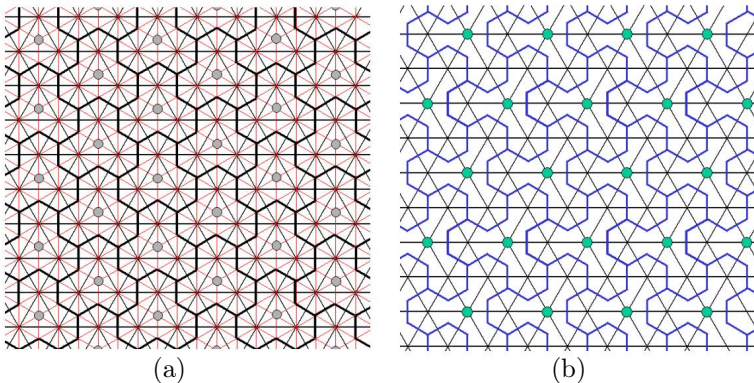


Fig. 3. Tiling the plane with polyhexes preserving symmetries: (a) a 3-hexe prototile centred at the junction point of three adjacent hexagons, (b) a 4-hexe prototile stabilizing the honeycomb symmetry.

4. The Niemeijer–van Leeuwen scaling picture

The “spin-cell” transformation is an important contribution of Niemeijer and van Leeuwen to the Kadanoff derivation of the scaling laws in the triangular lattice [21]. The transformation is again a subdivision of the spin system into “cells” assumed to interact in a similar way as the original spins. The cells are up(-pointing) triangles⁴ arranged in the original hexavalent lattice as shown in Fig. 4, where the sites of the new lattice, as centres of the triangles, form again a hexavalent lattice isomorphic to the original one;

⁴ Down(-pointing) in [22].

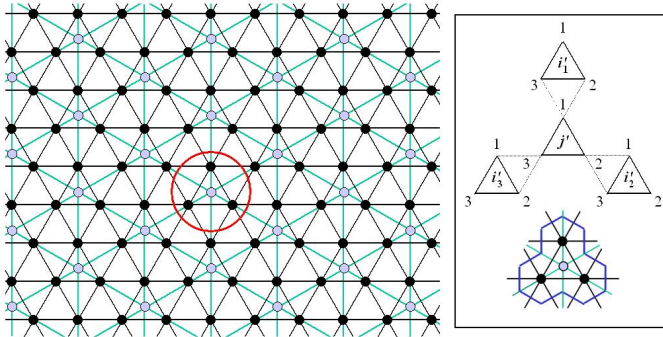


Fig. 4. Spin-cell transformation in the triangular lattice: the circle highlights a typical cell; a new lattice is induced by the transformation, whose sites are the centre of the cells. Inset: a pattern of nearest-neighbour intracell (in dotted lines) interactions; cells are labelled (j', i'_1, i'_2, i'_3) , sites are labelled $(1, 2, 3)$; beneath: the 3-hex prototile tiling the dual honeycomb in Fig. 3 (a).

the initial “lattice spacing”, or distance between neighbouring sites, is taken as unity. Periodic boundary conditions are considered with N sites in the thermodynamic limit $N \rightarrow \infty$.

The transformation from the site-spin Hamiltonian to a cell-spin Hamiltonian takes the general form

$$\mathcal{H}(s) = \sum_a K_a s_a \mapsto \mathcal{H}'(s') = \sum_{a'} K'_{a'} s'_{a'}, \tag{4.1}$$

$$s_a = \prod_{i \in a} s_i, \quad s'_{a'} = \prod_{i' \in a'} s'_{i'}, \tag{4.2}$$

where a runs through all subsets of sites i , a' runs through all subsets of cells i' , K_a and $K'_{a'}$ (in which temperature and Boltzmann constant are absorbed) are respectively the site–site interaction and the cell–cell interaction parameters and where $\{s\}$ (resp. $\{s'\}$) denotes the set of all site–spins (resp. cell–spins) configurations. The transformation $\mathcal{H}(s) \mapsto \mathcal{H}'(s')$ defines the renormalization operator and the ratio of homogeneity

$$\frac{N'}{N} = l^{-d}, \tag{4.3}$$

where N' stands for the number of cells, $d = 2$ the dimension of the lattice and l the stretch factor, should appear somehow like in Eq. (2.9). Evidently, the subdivision defines a partition of the vertex set as highlighted by the circle in Fig. 4, whence $l = \sqrt{3}$ and $3N' = N$. Note that the new lattice is rotated by $\pi/6$ and shifted by $\sqrt{3}/3$.

We focus now on how the edge set of the original lattice is organized. A perturbative approach is adopted, which splits the Hamiltonian into an unperturbed part \mathcal{H}^0 and a remainder \mathcal{V} as

$$\mathcal{H} = \mathcal{H}^0 + \mathcal{V}, \tag{4.4}$$

where intracell interactions are collected in \mathcal{H}^0 and intercell interactions in \mathcal{V} as

$$\mathcal{H}^0 = K \sum_{j'} \mathcal{H}_{j'}^0 = K \sum_{j'} (s_{j'}^1 s_{j'}^2 + s_{j'}^2 s_{j'}^3 + s_{j'}^3 s_{j'}^1) \tag{4.5}$$

$$\begin{aligned} \mathcal{V}_{i'_1 j'} &= K (s_{i'_1}^2 + s_{i'_1}^3) s_{j'}^1, \\ \mathcal{V}_{i'_2 j'} &= K (s_{i'_2}^3 + s_{i'_2}^1) s_{j'}^2, \\ \mathcal{V}_{i'_3 j'} &= K (s_{i'_3}^1 + s_{i'_3}^2) s_{j'}^3, \end{aligned} \tag{4.6}$$

over the whole lattice, where K is the nearest-neighbour coupling constant and according to the inset in Fig. 4: the superscript denotes the position of the site in the corresponding cell. The general expression of Hamiltonian in Eq. (4.1) with subsets $\{a, a'\}$ is justified by the authors, not only because they do not limit their study to a first-order perturbation but also because they extend it to a more sophisticated cluster approximation. As far as we are concerned we are strictly interested by the nearest-neighbour interactions, whence the expressions above with the simple factor K .

We finally check whether the construction really yields a partition of the edge set. For simplicity let

$$E(\mathcal{H}) = \{E(\mathcal{H}^0), E(\mathcal{V})\} \tag{4.7}$$

be the edge set induced by $\mathcal{H}^0 + \mathcal{V}$. Looking at the inset, we observe that the interaction patterns, related to “their” central cell j' are oriented towards, say, the N–SE–SW directions and therefore cannot overlap. Now, we enumerate three pairs of intercell bonds per cell according to Eq. (4.6), whence

$$|E(\mathcal{H})| = |E(\mathcal{H}^0)| + |E(\mathcal{V})| = 3N' + 6N' = 3N. \tag{4.8}$$

5. The arrowhead torus

A stepwise construction generated by the prototiling of Fig. 3 (b) can be iterated *ad infinitum* and has the property of being self-similar. The result is an *arrowhead* torus⁵ whose properties are examined hereafter. The inset

⁵ Whose name is borrowed from Mandelbrot for one of the self-similar Sierpiński figures [23].

in Fig. 5 highlights a reoriented N–SW–SE pattern of the 4-hex prototile, step two induces a tiling with a new prototile made of the union of four 4-hexes giving a 16-hex prototile.

A finite-size representation of the arrowhead is displayed on the left-hand side of Fig. 5, its hexagonal representation on the right side; both representations are isomorphic and we will only consider the hexagonal one in the sequel. The Sierpiński-like patchworks [24] highlight their recursive, hierarchical structure. As a Cayley graph, the arrowhead is vertex-transitive. The reader is referred to [25] for more details.

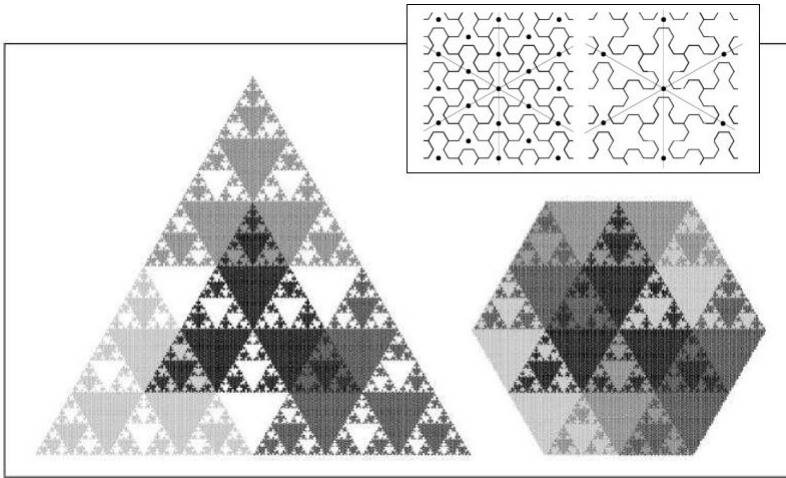


Fig. 5. Generic and hexagonal representation of an arrowhead of finite-size ($n = 8$) — inset: stepwise prototiling in the dual honeycomb for the first two steps.

Let $n \geq 0$ be the “size” of the arrowhead, denoted $\mathcal{AT}_n = (V_n, E_n)$. The order N of \mathcal{AT}_n is exactly $|V_n| = 4^n$ and the vertices are numbered in the set

$$I_n = \{0, 1, 2, \dots, 4^n - 1\} \tag{5.1}$$

according to a scheme resulting from the recursive construction of a finite-size torus within the infinite lattice. We denote by $I_1^* = \{1, 2, 3\}$ the generating set.

Since the arrowhead is 6-regular, its edge set cardinality is $|E_n| = 3N$. The connection scheme is defined as follows. Let X be any direction in the ordered set (N, SW, SE), let $(\delta_N, \delta_{SW}, \delta_{SE}) = (1, 2, 3)$ be the set of associated increments and \bar{X} be the opposite direction in (S, NE, NW) of X . Then

$${}^X\nu_0(0) = \bar{X}\nu_0(0) = 0 \tag{5.2}$$

and $\forall n \geq 1$

$${}^X\nu_n(4x) = 4x + \delta_X, \tag{5.3}$$

$$\overline{X}\nu_n(4x) = 4 \left(\overline{X}\nu_{n-1}(x) \right) + \delta_X, \tag{5.4}$$

where ${}^U\nu_k(u)$ denotes the neighbour in direction U of vertex u in \mathcal{AT}_k .

As an illustration and referring to Fig. 6, knowing the whole configuration of \mathcal{AT}_2 , let us examine which are the S, NE and NW neighbours of, say vertex 40, in \mathcal{AT}_3 :

$$\begin{aligned} {}^S\nu_3(40) &= 4 \left({}^S\nu_2(10) \right) + \delta_N = 4 \cdot 3 + 1 = 13 \\ {}^{\text{NE}}\nu_3(40) &= 4 \left({}^{\text{NE}}\nu_2(10) \right) + \delta_{\text{SW}} = 4 \cdot 8 + 2 = 34 \\ {}^{\text{NW}}\nu_3(40) &= 4 \left({}^{\text{NW}}\nu_2(10) \right) + \delta_{\text{SE}} = 4 \cdot 1 + 3 = 7. \end{aligned}$$

Incidentally, Fig. 6 which displays how is arranged the vertex set I_n in \mathcal{AT}_n and how it is induced by I_{n-1} gives also a rough insight on how a scale change can be organized. This construction is examined hereafter.

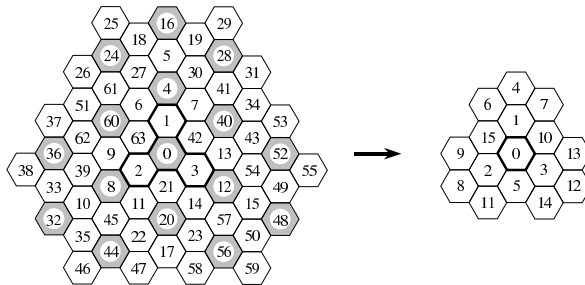


Fig. 6. Arrangement of the vertex set in \mathcal{AT}_n for $n = 3$ and its induced connection scheme. The pattern could also be viewed as a scale change by contraction of \mathcal{AT}_n into \mathcal{AT}_{n-1} : the centre of the 4-hexes is displayed in grey.

6. Scaling pictures in the arrowhead

6.1. Scaling a critical system

Starting from Kadanoff's picture in Sec. 2 and referring to the topology of the arrowhead, we suggest a new construction induced by the 4-hex of Fig. 3 (b). So given I_n in (5.1) we define the subset

$$I_{n,p} = \{x \in I_n : x \equiv 0 \pmod{4^p}\} \quad (0 \leq p \leq n) \tag{6.1}$$

of sites of I_n whose index is a multiple of 4^p . For any fixed p , a subset $I_{n,p}$ defines a subdivision of the lattice into 4^{n-p} blocks of size 4^p denoted by

$$\mathcal{B}_{n,p}(x) = \{x + i : i \in I_p\} \quad \forall x \in I_{n,p} \tag{6.2}$$

and whose site x having its index in $I_{n,p}$ is centre. Such a subdivision is highlighted in the inset of Fig. 5 for $p = 1$ and $p = 2$. In a stepwise renormalization, with nearest-neighbour interactions and following a first-order perturbative scheme, we are only interested by the case $p = 1$. So, for clarity's sake, we rewrite $I_{n,p}$ and $B_{n,p}$ as

$$I_{n,1} = \{x \in I_n : x \equiv 0 \pmod{4}\} \tag{6.3}$$

$$\mathcal{B}_{n,1}(x) = \{x + i : i \in I_1\} \quad \forall x \in I_{n,1} \tag{6.4}$$

as displayed in Fig. 7, where $I_{n,1}$ is the set of black sites and $\mathcal{B}_{n,1}(x)$ a 4-hexe enclosing the sites labelled $\{x, x + 1, x + 2, x + 3\}$ and arranged according to the N-SW-SE pattern. The number N_B of blocks $\mathcal{B}_{n,1}(x)$ is evidently $|I_{n,1}| = 4^{n-1}$.

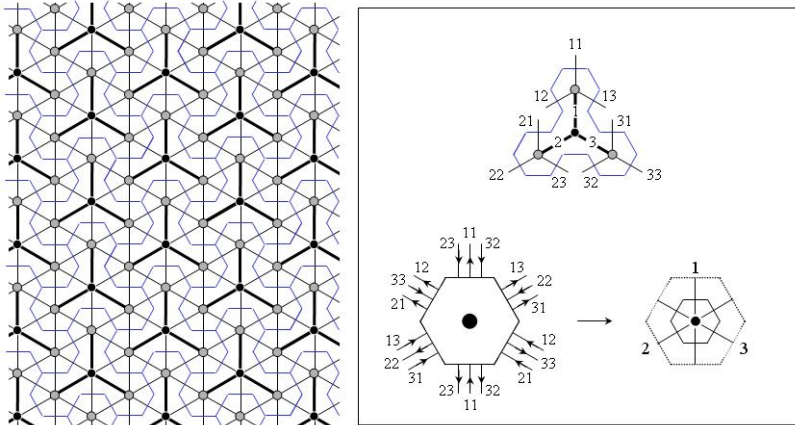


Fig. 7. Block subdivision, inner (in bold lines) and outer edges. Inset: labelling edges i_1 or i_1i_2 , respectively for inner and outer edges; beneath: the macrocell before and after contraction.

We now partition the edge set as follows. Let

$$I'_{n,1} = I_n - I_{n,1} \tag{6.5}$$

be the set of grey sites. E_n is partitioned into a subset E'_n of “inner bonds” within a block (in bold lines) and a subset E''_n of “outer bonds” between neighbouring blocks. Given $x \in I_{n,1}$ and $x' \in I'_{n,1}$, given two generators $i_1, i_2 \in I_1^* = \{1, 2, 3\}$:

- an inner edge (x, x') is labelled i_1 if x' is the i_1 -neighbour of x ,
- an outer edge (x', x'') is labelled i_1i_2 if x'' is the i_2 -neighbour of x' .

The detail is displayed in the upper part of the inset: $\{E'_n, E''_n\}$ is clearly a partition because all patterns have the form N–SW–SE hence cannot overlap and, on the other hand,

$$|E'_n| = 3N_B, \quad |E''_n| = 3|E'_n| \Rightarrow |E'_n| + |E''_n| = 12 \cdot 4^{n-1} = |E_n|. \tag{6.6}$$

The bottom part of the inset first shows a macrosite in the centre of a hexagonal macrocell with a stretch factor 2, yielding a new lattice whose vertex set is reduced to $I_{n,1}$. The contribution of a block $\mathcal{B}_{n,1}(x)$ to its six neighbours is emphasized by outgoing arcs, namely, three arcs such that $i_2 = i_1$ on the N–SW–SE pattern and three pairs with commuted labels $i_2 \neq i_1$ on the S–NE–NW pattern, that is, nine outgoing arcs altogether. Conversely, the contribution from its six neighbours is emphasized by incoming arcs according to a symmetrical pattern: evidently, two opposite directions N–S, SW–NE, SE–NW show the same label set.

Finally, the macrocell is contracted by a factor 2, giving a new, renormalized lattice $\tilde{\mathcal{A}}_n = (\tilde{V}_n, \tilde{E}_n)$ isomorphic to \mathcal{A}_{n-1} . Thus $I_{n,1}$ is mapped to I_{n-1} and since the contraction shrinks a block into a single “spin” and a triplet of outer bonds into a single “bond”, then

$$\tilde{E}'_n = \emptyset, \quad |\tilde{E}''_n| = \frac{1}{3}|E''_n| = |E'_n| = 3N_B = |E_{n-1}| \tag{6.7}$$

and finally

$$\tilde{V}_n \cong V_{n-1}, \quad \tilde{E}_n = \tilde{E}''_n \cong E_{n-1}. \tag{6.8}$$

According to the chosen N–SW–SE pattern, the edge set of the arrowhead could also be partitioned into three classes induced by the generator I_1^* . Therefore, in the hypothesis that no isotropy is assumed, the Hamiltonian might take the form

$$\mathcal{H} = K_1 \sum_{E_n^{(1)}} \sigma_{ij} \sigma_{i'j'} + K_2 \sum_{E_n^{(2)}} \sigma_{ij} \sigma_{i'j'} + K_3 \sum_{E_n^{(3)}} \sigma_{ij} \sigma_{i'j'}, \tag{6.9}$$

where K_1, K_2, K_3 would be the coupling constants associated to the respective subsets $E_n^{(1)}, E_n^{(2)}, E_n^{(3)}$ of E_n , induced by their generator in I_1^* .

Exploring the impact of the above picture upon the approximate exponents of a critical Ising system and, above all, upon the way to get them (or should it be otherwise) from an analysis similar to the Kadanoff or to the Niemeijer–van Leeuwen transformation is beyond the scope of this paper. Instead, we choose to forget criticality and, referring back to Introduction, to apply hereafter the scaling property of the arrowhead to *homogeneous* systems with a rather trivial example.

6.2. Scaling a large scale homogeneous system

Let us consider a sample representing a mixture made up of two phases ϕ_1 and ϕ_2 , mixed according to concentrations κ_1 and κ_2 with $\kappa_1 + \kappa_2 = 1$. By applying the above construction scheme, we plan to determine the correlation length ξ of a mesoscopic scale referred to a representative elementary volume (REV). At this scale, the mixture may be considered as homogeneous.

Let f_p be the occurrence frequency of phase ϕ_1 in a block of size 4^p ($0 \leq p \leq n$). For a given site, one has in particular $f_0 = 1$ if ϕ_1 is present in this site and $f_0 = 0$ otherwise. For a block of size 4^{p+1} , the frequency f_{p+1} follows from the recurrence relation

$$f_{p+1} = \psi(f_p) = \frac{1}{4} \sum_{i=0}^3 f_p^{(i)}, \quad (6.10)$$

where the $f_p^{(i)}$ denote the frequencies within each of the four corresponding sub-blocks labelled i in I_1 . Whenever the medium is globally homogeneous,

$$\forall \varepsilon > 0 \exists m \in \mathbb{N} : |f_{m+1} - f_m| \leq \varepsilon, \quad (6.11)$$

where ε is an arbitrary small real number (a divergence would occur otherwise). It follows from this that sequence $\{f_p\}$ is a Cauchy sequence which converges towards the finite limit

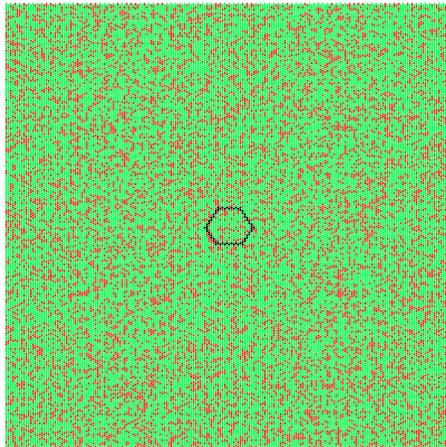


Fig. 8. Determination of a REV in a homogeneous mixture at the global scale with concentrations $\kappa_1 = 70\%$ and $\kappa_2 = 30\%$ (phase ϕ_1 appears in light grey). The pattern contains 40301 cells. The hexagonal polyhexe $B_{8,4}(0)$ contains 256 cells and defines a representative volume.

$$f^* = \psi(f^*) = \kappa_1. \tag{6.12}$$

This iterated construction leads to partition of the lattice into 4^{n-m} blocks of size 4^m , each of these blocks having the property of defining a representative volume of the whole mixture.

Fig. 8 displays a pattern⁶ of the mixture, covering about 40 000 cells and with concentrations $\kappa_1 = 70\%$ and $\kappa_2 = 30\%$, as well as a hexagonal block $B_{8,4}(0)$ entered in cell 0 and defining a representative volume of 256 cells. Table I details the convergence of the iterated sequence, ensured for $m = 4$ with accuracy $\varepsilon = 1\%$.

TABLE I

Convergence of the iterated sequence of frequencies, attained after 4 iterations with accuracy $\varepsilon = 1\%$.

f_0	1.00000
f_1	0.50000
f_2	0.68750
f_3	0.71875
f_4	0.70312
f_5	0.69922

7. Conclusion

Our contribution in this paper was to tackle the Kadanoff scaling picture and to embed it into the triangular lattice. A preliminary study on the various ways of prototiling the honeycomb tessellation has shown that only two patterns are relevant. The first one, constructed from a 3-hex prototile, had been investigated in detail by Niemeijer–van Leeuwen. First-order — nearest-neighbour — approximations were carried out to extract the critical exponents from the triangular Ising model according to the framework described in Sec. 4. Their work includes also a part of second-order approximations or more, as well as more sophisticated clustering approximations; this part was not tackled in this paper and the reader is referred again to [21, 22] for more details; in short, they observed that the accuracy of their approximation depends strongly upon the symmetry of the cluster. The other alternative, constructed from an “isotropic” 4-hex prototile is the core of our proposal. As far as we know, the resulting spin lattice has never been investigated elsewhere. Although the physical content of our proposal is reduced to its bare topological aspect, it is hoped yet that it would enable

⁶ In a network of size $n = 8$.

a shrewd reader to compare them. One can believe that the symmetry of this “arrowhead picture” might yield a better approximation of the universal critical exponents or at least bring out some simplified renormalization procedure to get them. The validity of our assumption is left to the reader’s attention as an open question.

I am indebted to Zoltán Rácz and Henk Hilhorst for motivating this preamble after having read a short and somewhat naive approach which should be viewed as an extended abstract.

REFERENCES

- [1] L.P. Kadanoff, *Physics* **2**, 263 (1966).
- [2] K.G. Wilson, J. Kogut, *Phys. Rep.* **12**, 75 (1974).
- [3] M.E. Fisher, *Rev. Mod. Phys.* **46**, 597 (1974).
- [4] S. Ma, *Rev. Mod. Phys.* **45**, 589 (1973).
- [5] H.E. Stanley, *Introduction to Phase Transitions and Critical Phenomena*, Oxford Univ. Press, London 1971.
- [6] W.D. McComb, *Renormalization Methods: a Guide for Beginners*, Oxford Univ. Press, 2004.
- [7] A. Lesne, *Renormalization Methods*, John Wiley and Sons, 1998.
- [8] M. Droz, *Invariance d’Échelle, Groupe de Renormalisation*, Univ. Genève, in preparation.
- [9] J.M. Ziman, *Models of Disorder: the Theoretical Physics of Homogeneously Disordered Systems*, Cambridge University Press, 1979.
- [10] S. Kirkpatrick, R.H. Swendsen, *Commun. ACM* **28**, 363 (1985).
- [11] R.J. Baxter, *Exactly Solved Models in Statistical Mechanics*, Academic Press, London 1982.
- [12] H.J. Hilhorst, M. Schick, J.M.J. van Leeuwen, *Phys. Rev.* **B19**, 2749 (1979).
- [13] D. Désérable, in 14th International Symp. of Math. Theory of Networks and Systems, MTNS 2000, Perpignan, France, 109 (2000).
- [14] S.W. Golomb, *J. Comb. Theory* **1**, 280 (1966).
- [15] B. Grünbaum, G.C Shephard, *Tilings and Patterns*, Freeman and Co., New York 1987.
- [16] C.K. Wong, D. Coppersmith, *J. ACM* **21**, 392 (1974).
- [17] F.K. Hwang, *Theor. Comput. Sci.* **299**, 107 (2003).
- [18] P. Morillo, M.A. Fiol, *Stochastica* **10**, 233 (1986).
- [19] P. Morillo, F. Comellas, M.A. Fiol, Technical Report 05-0286 (1986).
- [20] J.L. Yebra, M.A. Fiol, P. Morillo, I. Alegre, *Ars Combin.* **20B**, 159 (1985).

- [21] Th. Niemeijer, J.M.J. van Leeuwen, *Physica* **71**, 17 (1974).
- [22] Th. Niemeijer, J.M.J. van Leeuwen, *Phys. Rev. Lett.* **31**, 1411 (1973); also in [9].
- [23] B.B. Mandelbrot, *The Fractal Geometry of Nature*, Freeman and Cie, San Francisco 1982.
- [24] W. Sierpiński, *Prace Mat.-Fiz.* **27**, 77 (1916); *Acad. Pol. Sci.* **II**, 99 (1975).
- [25] D. Désérable, *Discrete Appl. Math.* **93**, 169 (1999).